Name of Journal: *World Journal of Gastroenterology*

Manuscript NO: 38594

Manuscript Type: Basic Research

Intra-individual comparison of therapeutic responses to vascular disrupting agent CA4P between rodent primary and secondary liver cancers

Yewei Liu[1,2,3,4], Frederik De Keyzer[2], Yuanbo Feng[2], Feng Chen[2], Shaoli Song[3], Johan Swinnen[2], Guy Bormans[2], Raymond Oyen[2], Gang Huang[1,3,4]*, Yicheng Ni[2]*

[1]Shanghai Key Laboratory for Molecular Imaging, Shanghai University of Medicine and Health Sciences, Shanghai 201318, China

[2]Biomedical Group, Campus Gasthuisberg, KU Leuven, Leuven 3000, Belgium

[3]Institute of Clinical Nuclear Medicine, Renji Hospital, Shanghai Jiao Tong University School of Medicine, Shanghai 200127, China

[4]Institute of Health Sciences, Shanghai Jiao Tong University School of Medicine (SJTUSM) & Shanghai Institutes for Biological Sciences (SIBS), Chinese Academy of Sciences (CAS), Shanghai 200025, China

Running title: **CA4P in rat primary and secondary liver cancers**

Correspondence to:

Yicheng Ni, MD, PhD. Theragnostic Laboratory, Department of Imaging and Pathology, Biomedical Group, KU Leuven, Herestraat 49, Leuven 3000, Belgium;
Email: yicheng.ni@kuleuven.be;
Tel: +32-16-330165; Fax: +32-16-343765

Abstract

AIM: To compare therapeutic responses of a vascular-disrupting-agent (VDA) Combretastatin-A4-phosphate (CA4P) among hepatocellular carcinomas (HCCs) and implanted rhabdomyosarcoma (R1) in the same rats by magnetic-resonance-imaging (MRI), microangiography and histopathology.

METHODS: Thirty-six HCCs were created by diethylnitrosamine gavaged in 14 rats that were also intrahepatically implanted with one R1 as monitored by T2-/T1-weighted images (T2WI/T1WI) on a 3.0T MRI-scanner. Vascular response and tumoral necrosis were detected by dynamic-contrast-enhanced (DCE-) and CE-MRI before, 1h and 12h after CA4P iv at 10 mg/kg (treatment group n=7) or PBS at 1.0 ml/kg (control group n=7). Tumor blood-supply was calculated by a semi-quantitative DCE parameter of area-under-the-time-signal-intensity-curve (AUC30). In vivo MRI findings were verified by postmortem techniques.

RESULTS: On CE-T1WIs, unlike the negative response in all tumors of control animals, in treatment group CA4P caused rapid extensive vascular shutdown in all R1-tumors, but mildly or spottily in HCCs at 1h. Consequently tumor necrosis occurred massively in R1-tumors but patchily in HCCs at 12h. AUC30 revealed vascular closure (66%) in R1-tumors at 1h ($P<0.05$), followed by further perfusion decrease at 12h ($P<0.01$); while less significant vascular clogging occurred in HCCs. Histomorphologically, CA4P induced more extensive necrosis in R1-tumors (92.6%) than in HCCs (50.2%) ($P<0.01$); tumor vascularity heterogeneously scored +~+++ in HCCs but homogeneously scored ++ in R1-tumors.

CONCLUSION: This study suggests superior performance of CA4P in metastatic over primary liver cancers, which could guide future clinical applications of VDAs.

Key words vascular-disrupting agent (VDA); combretastatin A4 phosphate (CA4P); hepatocellular carcinoma (HCC); rhabdomyosarcoma (R1); magnetic resonance imaging (MRI); rats

Core tip:

- Complex animal models combining primary and secondary liver malignancies proved feasible in rats.
- The therapeutic efficacy of the leading vascular disrupting agent CA4P could be intra-individually compared between primary and secondary liver malignancies in the same cirrhotic rats.
- Clinical 3.0T MRI allowed real-time monitoring of in vivo therapeutic responses within 12 hours, and ex vivo microangiography and histopathology could validate the CA4P-induced tumoricidal effects.
- The therapeutic responses appeared superior with secondary liver tumors over that with primary HCCs, which are of translational significance for planning future clinical trials of CA4P in cancer patients.

Liu Y, De Keyper F, Feng Y, Chen F, Song S, Swinnen J, Bormans G, Oyen R, Huang G, Ni Y. Intra-individual comparison of therapeutic responses to vascular disrupting agent CA4P between rodent primary and secondary liver cancers. *World J Gastroenterol* 2018; In press

Introduction

As a first vascular disrupting agent (VDA), combretastatin A4 phosphate (CA4P) targets the cytoskeletal tubulin of the abnormal tumor endothelial cells, leading to a rapid but often reversible vascular occlusion [1-3]. Theoretically, this may cause ischemic tumor necrosis by depriving malignant cells from blood supply [1-3]. Clinically CA4P has been undergoing phase II/III trials in the setting of ovarian, thyroid and lung cancers alone or in combination with other chemotherapeutic agents [4-6], and a good safety profile has also been shown in the first phase I clinical trial among Chinese patient population [7]. In the majority of transplanted tumor models, CA4P consistently induced massive central tumor necrosis, leaving only a few layers of peripheral viable tumor cells culpable for the incomplete treatment and cancer relapse [8, 9], which is also attributed to the unsatisfactory clinical outcomes [3]. To tackle this bottleneck problem with all VDAs, a plausible solution has been proposed [10].

On the other hand, diverse and paradoxical tumor responses to CA4P have been recently noticed in a few preclinical studies based on a carcinogen-induced primary liver cancer model [11, 12]. By gavage administration of diethylnitrosamine (DENA) in rodents, multifocal hepatomas of a full spectrum of tumor vascularity and cellular differentiation superimposed on various degrees of liver cirrhosis could be generated [11-14]. Compared with the ectopically and orthotopically transplanted tumors, this primary HCC model is considered to be more clinically relevant for evaluating therapeutic drugs because of the heterogeneity in tumoral microenvironment similar to that of humans [13, 14], if an imaging platform can be available to accurately trace individual tumors [14, 15]. In this model CA4P simultaneously caused not only tumor necrosis but also reginal parenchymal necrosis in the cirrhotic liver [11, 12].

Tumor susceptibility to VDA therapy could be largely influenced by vascular features such as vessel density, diameter, reginal instabilities in blood flow, vascular permeability and interstitial fluid pressure (IFP) [16, 17]. Evidences have shown that, rather than larger tumor vessels, smaller or thinner ones are more susceptible to completely shut down in response to VDAs [11, 12, 17]. Apart from the

intrinsic properties of tumor vasculature, different tumor implantation sites and their dissimilar host-organ blood-supplies may attribute to such variable efficacies of CA4P therapy as well [18, 19]. Take the ectopically implanted rhabdomyosarcoma (R1) as an example, intra-individual comparisons demonstrated that hepatic R1 tumors in the intact liver responded to CA4P much better than their subcutaneous and pancreatic counterparts did [18, 19]. However, issues still remain unknown as what if R1 tumors would grow in the cirrhotic liver, and whether R1 tumors growing in the cirrhotic liver are also good responders to CA4P as they presented in the normal liver [9, 10, 18-21].

So far experimentally on CA4P, all superior results in implanted liver tumors are derived from animals with healthy liver [9, 10, 18-21] and all inferior results on primary HCCs are from rats with liver cirrhosis [11]. Therefore, in order to assess this potential micro-environmental impact, it would be interesting to experimentally compare the therapeutic outcomes of CA4P between primary HCCs and secondary liver tumors in the same subjects with cirrhotic livers, though such a scenario is rarely seen in clinic [22]. Accordingly, in this study we employed a DENA-induced HCC model in WAG/Rij rats that received intrahepatic transplantation of a R1 tumor to intra-individually compare the responses of different tumors to CA4P administration under the same micro-environment of liver cirrhosis. A clinical 3.0T MRI was applied for in vivo real-time therapeutic monitoring within 12 hours, while ex vivo microangiography and histopathology were performed to validate the CA4P-induced outcomes.

Materials and Methods

Animals and reagents

Male Wistar Albino Glaxo/Rijswijk (WAG/Rij) rats, which are syngeneic for the cell-line of rhabdomyosarcoma (R1), weighting 300-350 g were purchased from Charles River Breeding Laboratories, Inc. (St. Aubain les Elbeuf, France). Diethylnitrosamine (DENA, N0258) was purchased from Sigma-Aldrich (St. Louis, MO, USA). Combretastatin A4 phosphate (CA4P, C643025) was procured from Toronto Research Chemical Inc. (Toronto, Canada). MRI contrast agent Dotarem® (Gd-DOTA, Gadoterate meglumine; Guerbet, France), barium sulfate suspension (Micropaque®, Guerbet, France) and gas anesthetic isoflurane (Forane®; Baxter Healthcare, Deerfield, IL) were also commercially obtained.

Experimental design

All animal experiments were approved by ethics committee of KU Leuven University and performed in compliance with European and national regulations. In vivo procedures including gavage feeding, drug injection and MR imaging were carried out under gas anesthesia with 2% isoflurane (Harvard Apparatus, Holliston, MA), while the laparotomy of intrahepatic R1 tumor implantation was carried out under general anesthesia with intraperitoneal injection of pentobarbital (Nembutal; Sanofi Sante Animale, Brussels, Belgium) at 50 mg/kg.

As illustrated in Figure 1, multifocal primary hepatomas superimposed on liver cirrhosis were induced in rats by 14-week oral gavage of DENA at 5 mg/kg/day using a 16 cm-long flexible plastic esophageal gastric tube (Fuchigami Kikai, Kyoto, Japan) [13]. Tumor growth was monitored weekly by T2WI and T1WI from the 9th week until the largest liver tumor diameter reached more than 5 mm. A R1 tumor tissue block of 1 mm^3 was implanted into the lower part of medium liver lobe by laparotomy. Tumor growth was monitored weekly by MRI until R1 reached more than 5 mm in diameter. Next, all recruited tumor-carrying rats were randomly divided into sham group and CA4P group. Seven rats in CA4P group were intravenously injected with CA4P at 10 mg/kg, while the other 7 rats in sham group intravenously received phosphate buffered saline (PBS) at 1ml/kg. Multi-

parametric MRI was performed 4 h before and 1 h and 12 h post CA4P/PBS treatment. Rats were sacrificed immediately after the last time point of MRI scanning for postmortem microangiography and histopathology.

In vivo MRI

A clinical 3.0T scanner (MAGNETOM Prisma; Siemens, Erlangen, Germany) and a human wrist coil (Hand/Wrist 16, A 3T Tim coil, Siemens) were used for imaging acquisition. To monitor tumor growth, T2-weighted (repetition time, 4000 ms; echo time, 70 ms; flip angle, 150°; field of view, 75×56 mm^2; matrix, 256×192; and acquisition time, 3.4 min) and T1-weighted (repetition time, 626 ms; echo time, 15 ms; flip angle, 160°; field of view, 75×56 mm^2; matrix, 256×192; and acquisition time, 3.8 min) turbo spin echo (TSE) images (T2WI, T1WI) were performed weekly. Sixteen axial images with a slice thickness of 2.2 mm and a gap of 0.4 mm were acquired. To evaluate tumor responses to CA4P treatment, T2WI, T1WI, Dynamic contrast enhanced (DCE) and consecutive CE-T1WIs were performed. DCE was conducted by a T1-weighted gradient echo (GE) sequence (repetition time, 7 ms; echo time, 2.45 ms; flip angle, 15°; field of view, 61×89 mm^2; and matrix, 132×192) with 60 measurements in total acquisition time of 7.3 min. During DCE, an intravenous bolus of 0.02 mmol/kg Gd-DOTA was injected after the first 17 precontrast baseline measurements that were continued with 43 postcontrast measurements. Then an intravenous bolus of 0.2 mmol/kg Gd-DOTA was injected, followed by consecutive CE-T1WI measurements.

MR Imaging analyses

Images were analyzed with an off-line Siemens workstation and MeVisLab (version 2.6.2, MeVis Medical Solutions AG, Bremen, Germany). All the following measurements were conducted by 3 authors with consensus.

1) Tumor diameter

On T2WI, the tumor was manually contoured on the lesion-containing slices and tumor volume was automatically generated by the software, on which the tumor diameter was obtained.

2) Semi-quantitative analysis of T1-weighted DCE

For DCE analysis namely AUC30 calculation, the operator-defined region of interest (ROI) of tumor was freehand delineated on all tumor-containing slices; ROI of abdominal aorta was delineated from 4 consecutive slices for defining arterial input function; ROI of the liver was delineated on 4 representative slices each from median, left, right and caudate lobes. All ROIs were automatically copied to all measurements. Because of a low gadolinium dose, a linear relation between the amount of contrast agent in the tissue and the resultant difference in relaxation time could been assumed [23]. As a robust semi-quantitative DCE parameter against movements, area under the time-signal intensity curve (AUC30) was calculated to reflect tumor blood flow [24].

Digital microangiography

After the last MRI scan, rats were anesthetized by an intraperitoneal injection of pentobarbital at 50 mg/kg. A laparotomy was performed with abdominal aorta cannulated, through which barium suspension was injected before the entire tumor-bearing liver was excised. Postmortem hepatic arteriography was conducted by a digital mammography unit (Em-brace; Agfa-Gevaert, Mortsel, Belgium) at 26 kV and 32 mAs. Then the livers were fixed and sliced into 3-mm sections in the axial plane corresponding to the MR images, before being radiographed at 26 kV and 18 mAs for qualitative validation of tumor vascularity.

Histopathology

After microangiography, the tissue sections were paraffin-imbedded, sliced and stained with hematoxylin and eosin (H&E) for microscopic analyses using an Axiovert 200M microscope equipped with an AxioCam MR monochrome digital camera (Carl Zeiss Inc, Gottingen, Germany) and AxioVision 4.8 software.

1) Calculation of CA4P-induced intratumoral necrosis

Microscopic images of H&E stained tumor slices at a magnification of 12.5 were used to estimate the percentage of intratumoral necrosis by using ImageJ software [25]. To get ‘necrotic ratio on each

section', ROIs around the entire tumor and the necrotic tumor were manually delineated, respectively. Sectional tumor area of each 3-mm tumor section was measured and represented as the axial slide representing this tumor block with the largest diameter. Tumor necrosis was estimated independently by 2 pathologists, and calculated with the equation: *Intratumoral necrosis ratio (%)* = $\sum$ *[Necrotic ratio on each section (%)* × *section area* (mm^2)*]* × *section thickness (mm) / [4/3π* r^3*]* (mm^3).

2) Grading of HCC differentiation

In view of the high analogy to histopathological feature in human liver cancer, rat HCCs were diagnosed according to the classical histomorphologic features: malignant hepatocytic tumors, often well vascularized, with wide trabeculae (> 3 cell layers), noticeable acinar pattern, small cell changes, cytologic atypia, prominent nucleoli, mitotic activity, vascular invasion, absence of Kupffer cells, the lack of portal triad, and the loss of the reticulin network [26]. The differentiation of rat HCCs was further graded using a modified 4-scale Edmondson and Steiner system [26] as the standard criteria: grade I, highly differentiated, consisting of tumor cells of moderate size arranged in thin trabeculae; grade II, larger cells with active nuclear mitosis and possible pseudoglandular structures often with steatosis; grade III, larger nuclei and more hyperchromatic or increased mitotic figures, granular and acidophilic cytoplasm, often with giant tumor cells; and grade IV, much less differentiated tumor cells with hyperchromatic nuclei and loss of trabecular pattern often with angioinvasion [26].

3) Grading of tumor vascularity

To characterize variable degrees of tumoral vascularity, a semi-quantitative vascular scoring system was adopted to classify HCCs as: (+) similar vascular density to the liver parenchyma; (++) dense vasculature without vascular lakes; (+++) denser vasculature with variously sized vascular lakes; and (++++) full of enlarged vascular lakes [11] [12].

Statistical analyses

Numerical data were expressed as the mean ± standard errors of the mean (SEM) and a significant difference was concluded for $P<0.05$. In vivo imaging biomarker AUC30 at different time points and

post-mortem tumoral necrosis were compared between HCC and liver R1 by unpaired two-tailed t-test using GraphPad Prism (version 7.02, GraphPad Software Inc, La Jolla, CA, USA).

Results

General aspects

In general, all rats tolerated well the experimental procedures including gas anesthesia, DENA gavage, MRI scanning, laparotomy of intrahepatic tumor implantation, contrast administration and intravenous CA4P/PBS treatment. In total, 19 primary HCCs and 7 hepatic R1 allografts were successfully established in the 7 rats of CA4P group (Table 1), while 17 primary HCCs and 7 R1 tumors were generated in the 7 rats of sham group. The rats were sacrificed 12 h after CA4P/PBS treatment when CA4P-induced tumor necrosis was most evident.

Uniform vs. variable vascularity between hepatic R1 allografts and primary HCCs

Similarly to the previous findings in Sprague Dawley (SD) rats [27], various tumoral vascularity and cellular differentiation of primary HCCs were discovered in WAG/Rij rats (Table 1). Yet vascularity of HCCs mainly appeared as grade +~++, probably due to a lower-dosed DENA gavage (5 mg vs. 10 mg/kg/day) but a prolonged administration period (150 d vs. 90 d) in addition to the different species. In contrast, vascularity of intrahepatic R1 allografts was uniformly identified as grade ++ (Table 1), similar to that of other tumor studies on different animal strains [9, 10, 18-21].

Tumoricidal effects in metastatic R1 tumors vs. heterogeneous responses in primary HCCs

In vivo real-time responses of primary HCCs and R1 allographs were visualized by multi-parametric MRI prior to, and 1 and 12 h post treatment. At baseline of CA4P group and all time points of sham group, hepatic R1 nodules appeared highly hyperintense on T2WIs (Fig. 2A1, 3A1, 2D1), iso- to slightly hyperinterse on precontrast T1WIs (Fig. 2A2, 3A2, 2D2) and homogeneously hyper-enhanced on CE-T1WIs (Fig. 2A3, 3A3, 2D3) compared with the liver parenchyma. Additionally, spontaneous necrosis existing in hepatic R1 of Rat 3 was indicated by the unenhanced area on CE-T1WI at baseline (Fig. 3A3). Intra-individually, their paired primary HCCs on the same imaging slice appeared moderately hyperintense on T2WIs (Fig. 2A1, 3A1, 2D1') as well as on precontrast T1WIs (Fig. 2A2, 3A2, 2D2'), and hyper-enhanced on CE-T1WIs (Fig. 2A3, 3A3, 2D3').

One hour after CA4P treatment, despite nearly unchanged intensities of hepatic R1 allographs on T2WIs (Fig. 2A1', 3A1') and T1WIs (Fig. 2A2', 3A2'), signals on CE-T1WIs distinctly altered by an unenhanced central region surrounded by a positively enhanced periphery (Fig. 2A3', 3A3'), indicative of ongoing extensive vascular shutdown. Nevertheless, the contrast of the primary HCC counterparts was slightly enhanced in a heterogeneous pattern (Fig. 2A3', 3A3').

Twelve hours later, massive central necrosis occurred in all the hepatic R1 tumors, as reflected by extremely hyperintense on T2WIs (Fig. 2A1''), isointense on T1WIs (Fig. 2A2'', 3A2'') and an unenhanced core surrounded by a hyperenhanced rim on CE-T1WIs (Fig. 2A3'', 3A3''). Meanwhile, By comparison, patchy necrosis was heterogeneously induced in primary HCCs, shown as generally increased hyperintensity on T2WIs (Fig. 2A1'', 3A1''), mingled hyper- and iso-intensities on T1WIs (Fig. 2A2'', 3A2'') and regional unenhancement scattering in extremely hyperenhanced lesions on CE-T1WIs (Fig. 2A3'', 3A3'').

These in vivo imaging findings were eventually confirmed by postmortem microangiography and histopathology. At 12 h, complete absence of tumor vessels was particularly identified in the center of hepatic R1 (Fig. 2B, 3B), whereas in primary HCCs, generally denser vasculature was mixed with patchy avascular areas (Fig. 2B, 3B). From H&E stained slices, massive hemorrhagic necrosis and focal necrosis were indicated in hepatic R1 and in primary HCCs, respectively (Fig. 2C, 3C).

Meanwhile, in the sham group (Fig. 2D), in vivo MRI did not show any obvious difference 4 h before, and 1 and 12 h after PBS injection. From postmortems, no vascular changes were microangiographically identified, and no acute tumoral necrosis was histopathologically discovered.

Quantitative changes of tumor blood supply in correlation to CA4P-induced necrosis

Real-time changes of tumor blood supply after CA4P administration were monitored by in vivo DCE-MRI. As reflected by AUC30 (Fig. 4A), blood flow in hepatic R1 tumors dropped by 66% at 1 h due to vascular shut-down, followed by a further reduction of 7.3% at 12 h as a result of massive

tumoral necrosis (Fig. 4B). Nevertheless, in primary HCCs, only 11% tumor blood flow was reduced at 1 h because of vascular clogging, followed by a slight resume of tumor perfusion at 12 h (Fig. 4B), which was a heterogeneous combination of partial tumoral necrosis and re-opening of large intratumoral vessels in residual tumor. As validated by histopathological analysis, tumoral necrosis in liver R1 allographs (92.6%) was more extensive than that in primary HCCs (50.2%) at 12 h after CA4P treatment (Fig. 4C, Table 1).

Taken together, these intraindividual comparisons demonstrated that in generally CA4P caused more extensive tumor vascular destruction and consequent tumoral necrosis in intrahepatically implanted R1 tumors than in the primary HCC lesions, both under the same cirrhotic liver background.

Discussion

To the best of our knowledge, this is the first study where 1) a rat tumor model combining primary HCCs and an implanted R1 tumor in the same cirrhotic liver has thus been established; and 2) the therapeutic efficacies of a VDA CA4P on distinct tumor types have been intra-individually compared. This, together with the applied MRI-microangiography-histology platform, could be regarded as methodological advances for conducting more efficient theragnostic investigations on spontaneous versus metastatic liver malignancies.

This unique rat model of primary and secondary liver tumors induced by a carcinogen and surgery was employed not only to closely mimic the synchronous primary and metastatic liver malignancies seen in clinical patients, though of rarity [22], but also to better compare such complex liver cancers, especially in terms of different tumor differentiation, angiogenesis and vasculature, towards the same therapeutics of CA4P.

Based on the fact that the target of CA4P is tumoral vasculature rather than cancer cells, transplanted R1 rhabodomyosarcoma is a suitable model of secondary hepatic tumor because of the similar tumor neovascularization process and the existing vasculature pattern to those intrahepatic metastases [15]. Transplanted R1 tumor is a type of homogeneous, hypervascularized, soild tumor, with abundant

micro-vessels[14]. Although in patients intrahepatic metastases occur via hematogenous route, they always end up with the same consequence of tumor neovascularization. Therefore, the derived results are representative of that in other metastatic liver tumors from different original sites.

Unlike ectopically and orthotopically transplanted tumor models that yield reproducible outcomes, experimental models of primary liver malignancies tend to be more therapeutically and histologically unpredictable owing to intra- and intertumoral heterogeneity [11, 12]. Particularly, despite undergoing similar carcinogenesis, DENA-induced primary HCCs exhibit huge diversities in carcinoma development, neovascularization or tumor vascularity, microenvironment, and cellular differentiation in addition to varied degrees of liver cirrhosis [11, 12, 14]. Therefore, while constructing both primary and implanted tumors could be more time-consuming and technically challenging [13], this complex liver tumor model appears more clinically relevant for mimicking miscellaneous human cancers [14, 22].

In this study, distinct responses to CA4P, namely more complete tumoricidal effect on implanted R1 tumors versus variable outcomes in primary HCCs, simultaneously occurred in the same rats with cirrhotic livers. These findings are in alignment with the previous studies conducted in either DENA-induced primary HCC model on cirrhotic liver [11, 12] or implanted R1 tumor model in normal liver [9, 10, 20, 21]. Thus, the role of cirrhotic or normal liver background in the therapeutic impact of CA4P could be basically excluded. It was more likely that the intrinsic vasculature of the individual tumors eventually determined various outcomes of CA4P therapy. Indeed, as a widely accepted notion, implanted liver tumors resemble more closely to the secondary or metastatic liver cancer [15]. Therefore, our results strongly indicate that in general CA4P exerts more potent therapeutic effects on the metastatic liver tumors, rather than the primary liver tumors.

In principle, tumor angiogenesis switches on when tumor reaches 1 mm^3 in volume, since this is the limited size of diffusion within which solid tumor cells can grow [28]. Apart from the basic type of angiogenesis, namely endothelial sprouting, there are several nonangiogenic tumor vascularization

mechanisms including vasculogenic mimicry (VM), intussusception and vascular co-option [29, 30]. VM refers to tumor cells mimicking endothelial cells and directly participating in blood vessel formation, while intussusception and vascular co-option are both vascularization modes that essentially take advantage of the existing vasculature in the surrounding benign tissue [29, 30]. For instance, in experimental liver metastatic model produced by splenic injection of CD38 colon carcinoma cells in mice, enlarged sinusoidal lakes were discovered to be developed by fusion of the normal structure of sinusoids [31]. Since primary HCCs are generally hypervascularized tumors [32], vascularization based on remodeling the existing blood vessels is more complicated, especially in terms of enlarged vascular lakes. These evidences may to some extent explain the heterogeneous vasculature observed in our primary HCC model that developed gradually in the context of cirrhotic liver [11]. Supportively, by treating rats with DENA in a lower dose and a longer exposure period, less severe liver cirrhosis along with lower grades of tumor vascularity and HCC differentiation were identified in this study as compared to a previous study [11].

Liver cirrhosis is considered as a precancerous condition since over 80% HCCs arise on a background of cirrhosis [26, 33]. In fact, the progression of cirrhosis is accompanied by a deformation of the hepatic vasculature in regenerated lobules [34]. Consequent hepatic vascular alterations include shunting of the portal and arterial blood directly into the central vein, compromising exchange between hepatic sinusoids and the adjacent liver parenchyma, and disturbed hepatobiliary excretion [32] [34]. In the context of cirrhosis, distorted neovasculature not only function as a unique mode of blood supply, but also appeared to be responsive to CA4P treatment, leading to patchy necrosis in cirrhotic liver paranchyma [12]. Hence, vigilance should be exercised when using VDAs upon patients with extensive liver cirrhosis, since acute necrosis in liver parenchyma could further impair hepatic function.

Currently, although a series of phase II/III clinical trials have aimed at evaluating the treatment of CA4P in combination with chemotherapy in ovarian cancer [4], anaplastic thyroid cancer [5] and

nonsquamous non-small cell lung cancer patients [6], CA4P still literally remains an investigational medicine. The fetter that prevents CA4P from being ultimately adopted as a clinical anti-cancer therapy lies in tumor regrowth after monotherapy [35], despite its prompt, effective and generic responses in almost all solid tumors. Hence, combining CA4P with sequential treatments like chemotherapy, conventional radiotherapy, internal targeted radiotherapy and antiangiogenic therapy could reinvigorate these VDAs and provide better long-term outcomes. In fact, a dual-targeting pan-anticancer theragnostic approach called OncoCiDia using CA4P sequentially with a radioiodinated necrosis avid compound ^{131}I-Hypericin has been proposed to achieve CA4P-induced necrosis-oriented internal targeted radiotherapy [10, 36]. In this context, prior to setting a serial VDA-centric anti-cancer protocols, the present synchronous multiple liver cancer model in rodents could be a stepping-stone to help predict the diverse responses that may occur in patients, and to further address more complicated clinically relevant questions [22]. For instance, to those patients with the HCCs less responsive to CA4P, alternatives such as radiofrequency ablation (RFA), microwave ablation (MW) and high intensity focused ultrasound (HIFU) can be applied to massively necrotize the tumor before systemic administration of a necrosis-avid radiopharmaceutical in the OncoCiDia strategy [10, 36].

Conclusions

This study suggests distinct responses to CA4P, namely more complete tumoricidal effect on implanted R1 tumors versus variable outcomes in primary HCCs, simultaneously occurred in the same rats with cirrhotic livers, which could help to guide future clinical applications of VDAs.

Abbreviations

CA4P: combretastatin A4 phosphate

HCC: hepatocellular carcinoma

MRI: magnetic resonance imaging

DENA: diethylnitrosamine

T2WI: T2-weighted imaging

T1WI: T1-weighted imaging

DCE- MRI: dynamic contrast enhanced MRI

CE-MRI: contrast-enhanced MRI

AUC30: area under the time-signal intensity curve

VDA: vascular-disrupting agent

IFP: interstitial fluid pressure

WAG/Rij rats: Wistar Albino Glaxo/Rijswijk rats

TSE: turbo spin echo turbo spin echo

EPI: echo-planar imaging

GE: gradient echo

ROI: region of interest

H&E: hematoxylin and eosin

SEM: standard errors of the mean

SD rats: Sprague Dawley rats

VM: vasculogenic mimic

Ethics Committee Approval

This animal experiment was performed in compliance with European and national regulations after approval by KU Leuven university ethics committee (P147/2013) for animal care and use.

ARTICLE HIGHLIGHTS

Research background

Previously, all favorable responses to the vascular-disrupting-agent (VDA) Combretastatin-A4-phosphate (CA4P) on implanted liver tumors are derived from animals with healthy liver. Yet the diverse and paradoxical responses to CA4P on primary hepatomas are from rats with cirrhotic liver.

Research motivation

Therapeutic responses of CA4P between primary and secondary hepatic tumors had never been compared intraindividually in the same rats with underlying liver cirrhosis. And the potential micro-environmental impact from the surrounding liver parenchyma needed to be further assessed.

Research objectives

We aimed to compare therapeutic responses of CA4P among carcinogen-induced primary hepatocellular carcinomas (HCCs) and surgically implanted rhabdomyosarcoma (R1) in the same rats by magnetic-resonance-imaging (MRI), microangiography and histopathology.

Research methods

We performed diethylnitrosamine (DENA) gavage to induce primary HCCs and meanwhile intrahepatic implantation of R1 to create secondary liver tumor in the same rats. Tumor growth was monitored by T2-/T1-weighted images on a 3.0T MRI-scanner. Rats were then intravenously treated with CA4P. Vascular response and tumoral necrosis before and after treatment were compared by dynamic-contrast-enhanced (DCE-) and CE-MRI. Tumor blood supply was further calculated by a semi-quantitative DCE parameter of area-under-the-time-signal-intensity-curve (AUC30). Eventually in vivo MR imaging findings were validated by postmortem techniques.

Research results

In total, 19 primary HCCs and 7 hepatic R1 allografts were successfully established in the 7 rats of CA4P group, while 17 primary HCCs and 7 R1 tumors were generated in the 7 rats of sham group. Uniform and variable vascularity were identified, respectively, in hepatic R1 allografts and primary HCCs. As documented by in vivo MRI and post-mortem histopathology, vascular shutdown generally occurred at 1 hour after CA4P treatment; 12 hours later, tumoricidal effects were observed in secondary R1 tumors, while heterogeneous responses were seen in the primary HCCs. Quantitatively, tumor blood supply reflected by AUC30 showed vascular closure (66%) in R1-tumors at 1h ($P<0.05$), followed by further perfusion decrease at 12h ($P<0.01$); while less significant vascular clogging occurred in HCCs. Histomorphologically, CA4P induced more extensive necrosis in R1-tumors (92.6%) than in HCCs (50.2%) ($P<0.01$); tumor vascularity heterogeneously scored +~+++ in HCCs but homogeneously scored ++ in R1-tumors.

Research conclusions

To verify our original hypothesis that primary and secondary liver cancers may respond differently to VDA therapy due to the dissimilar tumor vascularity, a complex rat tumor model combining carcinogen-induced primary HCCs and a surgically implanted R1 tumor in the same cirrhotic rats has thus been established to compare CA4P therapeutic responses intraindividually under the same micro-environment. Indeed, our hypothesis was verified by the superior performance of CA4P in metastatic over primary liver cancers. This could help to design future clinical trials and guide applications of VDAs.

Research perspectives

The merit of this study is that the present synchronous multiple liver cancer model in rodents could be a stepping-stone to help predict the diverse responses that may occur in patients, and to further address more complicated clinically relevant questions. The lesson that could be learnt from this study lies in, although HCCs are generally hypervascularized, we should not take it for granted that

the rich abnormal blood vessels naturally serve as plenty of drug targets for the VDA to inevitably induce massive tumor necrosis. This preclinical study is for preparing a novel dual targeting pan-anticancer theragnostic strategy OncoCiDia in human liver cancers where CA4P could be applied as the first step.

References

1. Tozer GM, Kanthou C, Baguley BC. Disrupting tumour blood vessels. *Nat Rev Cancer* 2005;**5**:423–35 [PMID: 15928673 DOI: 10.1038/nrc1628]
2. Cooney MM, van Heeckeren W, Bhakta S, Ortiz J, Remick SC. Drug Insight: vascular disrupting agents and angiogenesis—novel approaches for drug delivery. *Nat Clin Pract Oncol* 2006;**3**:682–92 [PMID: 17139319 DOI: 10.1038/ncponc0663]
3. Siemann DW, Chaplin DJ, Walicke PA. A review and update of the current status of the vasculature disabling agent combretastatin-A4-phosphate (CA4P). *Expert Opin Investig Drugs* 2009;**18**:189–97 [PMID: 19236265 DOI: 10.1517/13543780802691068]
4. Zweifel M, Jayson GC, Reed NS, Osborne R, Hassan B, Ledermann J, Shreeves G, Poupard L, Lu S-P, Balkissoon J, Chaplin DJ, Rustin GJS. Phase II trial of combretastatin A4 phosphate, carboplatin, and paclitaxel in patients with platinum-resistant ovarian cancer. *Ann Oncol* 2011;**22**:2036–41 [PMID: 21273348 DOI: 10.1093/annonc/mdq708]
5. Sosa JA, Elisei R, Jarzab B, Bal CS, Koussis H, Gramza AW, Ben-Yosef R, Gitlitz BJ, Haugen B, Karandikar SM, Khuri FR, Licitra LF, Remick SC, Marur S, Lu C, Ondrey FG, Lu S, Balkissoon J. A randomized phase II/III trial of a tumor vascular disrupting agent fosbretabulin tromethamine (CA4P) with carboplatin (C) and paclitaxel (P) in anaplastic thyroid cancer (ATC): Final survival analysis for the FACT trial. *J Clin Oncol* 2011;**29**:5502–5502 [DOI: 10.1200/jco.2011.29.15_suppl.5502]
6. Garon EB, Kabbinavar FF, Neidhart JA, Neidhart JD, Gabrail NY, Oliveira MR, Lu SP, Balkissoon J. Randomized phase II trial of a tumor vascular disrupting agent fosbretabulin tromethamine (CA4P) with carboplatin (C), paclitaxel (P), and bevacizumab (B) in stage IIIb/IV nonsquamous non-small cell lung cancer (NSCLC): The FALCON trial. *J Clin Oncol* 2010;**28**:7587–7587 [DOI: 10.1200/jco.2010.28.15_suppl.7587]
7. He X, Li S, Huang H, Li Z, Chen L, Ye S, Huang J, Zhan J, Lin T. A pharmacokinetic and safety study of single dose intravenous combretastatin A4 phosphate in Chinese patients with

refractory solid tumours. *Br J Clin Pharmacol* 2011;**71**:860–70 [PMID: 21276042 DOI: 10.1111/j.1365-2125.2011.03928.x]

8. Grosios K, Holwell SE, McGown AT, Pettit GR, Bibby MC. In vivo and in vitro evaluation of combretastatin A-4 and its sodium phosphate prodrug. *Br J Cancer* 1999;**81**:1318–27 [PMID: 10604728 DOI: 10.1038/sj.bjc.6692174]
9. Wang H, Li J, Chen F, Keyzer F, Yu J, Feng Y, Nuyts J, Marchal G, Ni Y. Morphological, functional and metabolic imaging biomarkers: assessment of vascular-disrupting effect on rodent liver tumours. *Eur Radiol* 2010;**20**:2013–26 [PMID: 20182730 DOI: 10.1007/s00330-010-1743-5]
10. Li J, Sun Z, Zhang J, Shao H, Cona MM, Wang H, Marysael T, Chen F, Prinsen K, Zhou L, Huang D, Nuyts J, Yu J, Meng B, Bormans G, Fang Z, de Witte P, Li Y, Verbruggen A, Wang X, Mortelmans L, Xu K, Marchal G, Ni Y. A dual-targeting anticancer approach: soil and seed principle. *Radiology* 2011;**260**:799–807 [PMID: 21712473 DOI: 10.1148/radiol.11102120]
11. Liu Y, De Keyzer F, Wang Y, Wang F, Feng Y, Chen F, Yu J, Liu J, Song S, Swinnen J, Bormans G, Oyen R, Huang G, Ni Y. The first study on therapeutic efficacies of a vascular disrupting agent CA4P among primary hepatocellular carcinomas with a full spectrum of differentiation and vascularity: correlation of MRI-microangiography-histopathology in rats. *Int J Cancer* 2018 (accepted)
12. Liu Y, Yin T, Keyzer FD, Feng Y, Chen F, Liu J, Song S, Yu J, Vandecaveye V, Swinnen J, Bormans G, Himmelreich U, Oyen R, Zhang J, Huang G, Ni Y. Micro-HCCs in rats with liver cirrhosis: paradoxical targeting effects with vascular disrupting agent CA4P. *Oncotarget* 2017;**8**:55204–15 [PMID: 28903414 DOI: 10.18632/oncotarget.19339]
13. Liu Y, Yin T, Feng Y, Cona MM, Huang G, Liu J, Song S, Jiang Y, Xia Q, Swinnen JV, Bormans G, Himmelreich U, Oyen R, Ni Y. Mammalian models of chemically induced primary malignancies exploitable for imaging-based preclinical theragnostic research. *Quant Imaging Med Surg* 2015;**5**:708–29 [PMID: 26682141 DOI: 10.3978/j.issn.2223-4292.2015.06.01]

14. Ni Y, Marchal G, Yu J, Mühler A, Lukito G, Baert AL. Prolonged positive contrast enhancement with Gd-EOB-DTPA in experimental liver tumors: Potential value in tissue characterization. *J Magn Reson Imaging* 1994;**4**:355–63 [PMID: 8061434 DOI: 10.1002/jmri.1880040322]

15. Ni Y, Wang H, Chen F, Li J, DeKeyzer F, Feng Y, Yu J, Bosmans H, Marchal G. Tumor models and specific contrast agents for small animal imaging in oncology. *Methods* 2009;**48**:125–38 [DOI: 10.1016/j.ymeth.2009.03.014]

16. Tozer GM, Kanthou C, Lewis G, Prise VE, Vojnovic B, Hill SA. Tumour vascular disrupting agents: combating treatment resistance. *Br J Radiol* 2008;**81**:S12–20 [PMID: 18819993 DOI: 10.1259/bjr/36205483]

17. Wu X-Y, Ma W, Gurung K, Guo C-H. Mechanisms of tumor resistance to small-molecule vascular disrupting agents: Treatment and rationale of combination therapy. *J Formos Med Assoc* 2013;**112**:115–24 [PMID: 23473523 DOI: 10.1016/j.jfma.2012.09.017]

18. Li J, Chen F, Feng Y, Cona MM, Yu J, Verbruggen A, Zhang J, Oyen R, Ni Y. Diverse responses to vascular disrupting agent combretastatin A4 phosphate: a comparative study in rats with hepatic and subcutaneous tumor allografts using MRI biomarkers, microangiography, and histopathology. *Transl Oncol* 2013;**6**:42–50 [PMID: 23418616 DOI: 10.1593/tlo.12367]

19. Yin T, Liu Y, Peeters R, Feng Y, Yu J, Himmelreich U, Oyen R, Ni Y. Vascular disrupting agent in pancreatic and hepatic tumour allografts: observations of location-dependent efficacy by MRI, microangiography and histomorphology. *Br J Cancer* 2017;**117**:1529–36 [PMID: 28910821 DOI: 10.1038/bjc.2017.324]

20. Wang H, Van de Putte M, Chen F, De Keyzer F, Jin L, Yu J, Marchal G, de Witte P, Ni Y. Murine liver implantation of radiation-induced fibrosarcoma: characterization with MR imaging, microangiography and histopathology. *Eur Radiol* 2008;**18**:1422–30 [PMID: 18343928 DOI: 10.1007/s00330-008-0904-2]

21. Wang H, Sun X, Chen F, De Keyzer F, Yu J, Landuyt W, Vandecaveye V, Peeters R, Bosmans H, Hermans R, Marchal G, Ni Y. Treatment of rodent liver tumor with combretastatin a4 phosphate: noninvasive therapeutic evaluation using multiparametric magnetic resonance imaging in correlation with microangiography and histology. *Invest Radiol* 2009;**44**:44–53 [PMID: 19034028 DOI: 10.1097/RLI.0b013e31818e5ace]

22. Maida M, Macaluso FS, Galia M, Cabibbo G. Hepatocellular carcinoma and synchronous liver metastases from colorectal cancer in cirrhosis: A case report. *World J Hepatol* 2013;**5**:696–700 [PMID: 24409337 DOI: 10.4254/wjh.v5.i12.696]

23. Tofts PS, Berkowitz BA. Rapid measurement of capillary permeability using the early part of the dynamic Gd-DTPA MRI enhancement curve. *J Magn Reson B* 1993;**102**:129–36 [DOI: 10.1006/jmrb.1993.1075]

24. Yankeelov TE, Gore JC. Dynamic contrast enhanced magnetic resonance imaging in oncology: theory, data acquisition, analysis, and examples. *Curr Med Imaging Rev* 2009;**3**:91–107 [PMID: 19829742 DOI: 10.2174/157340507780619179]

25. Buijs M, Vossen JA, Geschwind J-FH, Salibi N, Pan L, Ventura VP, Liapi E, Lee KH, Kamel IR. Quantitative Proton MR Spectroscopy as a Biomarker of Tumor Necrosis in the Rabbit VX2 Liver Tumor. *J Vasc Interv Radiol JVIR* 2011;**22**:1175–80 [PMID: 21620723 DOI: 10.1016/j.jvir.2011.03.016]

26. Schlageter M, Terracciano LM, D'Angelo S, Sorrentino P. Histopathology of hepatocellular carcinoma. *World J Gastroenterol WJG* 2014;**20**:15955–64 [PMID: 25473149 DOI: 10.3748/wjg.v20.i43.15955]

27. Ni Y, Marchal G, Vandamme B, Vanhecke P, Michiels J, Zhang X, Yu J, Baert A. Magnetic Resonance Imaging, Microangiography, and Histology in a Rat Model of Primary Liver-Cancer. *Invest Radiol* 1992;**27**:689–97 [DOI: 10.1097/00004424-199209000-00006]

28. Folkman J, Cotran R. Relation of vascular proliferation to tumor growth. *Int Rev Exp Pathol* 1976;**16**:207–48 [PMID: 783062]

29. Donnem T, Hu J, Ferguson M, Adighibe O, Snell C, Harris AL, Gatter KC, Pezzella F. Vessel co-option in primary human tumors and metastases: an obstacle to effective anti-angiogenic treatment? *Cancer Med* 2013;**2**:427–36 [PMID: 24156015 DOI: 10.1002/cam4.105]

30. Bugyik E, Renyi-Vamos F, Szabo V, Dezso K, Ecker N, Rokusz A, Nagy P, Dome B, Paku S. Mechanisms of vascularization in murine models of primary and metastatic tumor growth. *Chin J Cancer* 2016;**35** [PMID: 26873579 DOI: 10.1186/s40880-016-0083-5]

31. Paku S, Kopper L, Nagy P. Development of the vasculature in "pushing-type" liver metastases of an experimental colorectal cancer. *Int J Cancer* 2005;**115**:893–902 [DOI: 10.1002/ijc.20886]

32. Yang ZF, Poon RTP. Vascular changes in hepatocellular carcinoma. *Anat Rec Hoboken NJ 2007* 2008;**291**:721–34 [PMID: 18484619 DOI: 10.1002/ar.20668]

33. Maier KP. Cirrhosis of the liver as a precancerous condition. *Praxis* 1998;**87**:1462–5 [PMID: 9847685]

34. Schuppan D, Afdhal NH. Liver Cirrhosis. *Lancet* 2008;**371**:838–51 [PMID: 18328931 DOI: 10.1016/S0140-6736(08)60383-9]

35. Li J, Cona MM, Chen F, Feng Y, Zhou L, Yu J, Nuyts J, de Witte P, Zhang J, Himmelreich U, Verbruggen A, Ni Y. Exploring theranostic potentials of radioiodinated hypericin in rodent necrosis models. *Theranostics* 2012;**2**:1010–9 [DOI: 10.7150/thno.4924]

36. Ni Y. Abstract 1767: Oncocidia: a small molecule dual targeting pan-anticancer theragnostic strategy. Cancer Res 2014;**74**:1767–1767 [DOI: 10.1158/1538-7445.AM2014-1767]

Table 1. Intra-individual comparison of induced tumor necrosis (%) between primary HCCs and intrahepatically implanted R1 rhabdomyosarcomas in CA4P-treated group

	Primary HCC					Implanted hepatic R1			
Rat	**Tumor code**	**CA4P-induced necrosis (%)**	**Tumor diameter (mm)**	**Tumor vascularity ***	**Tumor differentiation ****	**Tumor code**	**CA4P-induced necrosis (%)**	**Tumor diameter (mm)**	**Tumor vascularity ***
1	**HCC_1**	21.8	9.7	++	II	**R1_1**	72.3	12.1	++
	HCC_2	16.4	6.5	++	III~IV				
	HCC_3	0	10.9	++	III				
2	**HCC_4**	43.1	6.4	+	III	**R1_2**	84.5	12.6	++
	HCC_5	23.3	8.5	++	III				
3	**HCC_6**	92.3	8.1	+ *	I~II	**R1_3**	99.2	10	++
	HCC_7	96.5	6.2	+ *	II				
	HCC_8	19.8	10	+	I				
	HCC_9	98.9	10	+	II				
4	**HCC_10**	99.2	14.3	+ *	I~II	**R1_4**	96.8	9.8	++
5	**HCC_11**	27.6	18.3	+	III	**R1_5**	99.4	8.3	++
	HCC_12	4.9	7.8	++	II~III				
	HCC_13	62.7	13	+	I~II				
6	**HCC_14**	47.6	14.2	+, +++ ***	I, III ****	**R1_6**	97.7	9	++
	HCC_15	46.4	14.2	+, +++ ***	I, III ****				
7	**HCC_16**	76.1	12.5	+ *	II~III	**R1_7**	98.3	6.2	++
	HCC_17	52.6	11.9	+	III				
	HCC_18	33.4	10.4	+	III				
	HCC_19	91.2	9	+ *	I~II				
Mean ± SD		50.2 ± 1.8	10.6 ± 0.2	/	/		92.6 ± 1.5	9.7 ± 0.3	/

Note:

* A vascular scoring system for rat liver tumor: vascular density similar to that of liver parenchyma (+), denser vasculature without vascular lakes (++), denser vasculature with small-sized vascular lakes (+++), and full of large vascular lakes (++++).

** A 4-scale grading system for HCC differentiation in rats: well (I), moderately (II), poorly (III) and un-(IV) differentiated HCC lesions.

*** Tumor vascularity was graded as + in the necrotic tumor, and +++ in the residual viable part.

**** HCC differentiation was scored by I in the necrotic tumor, and III in the residual viable part.

Figures and Figure Legends

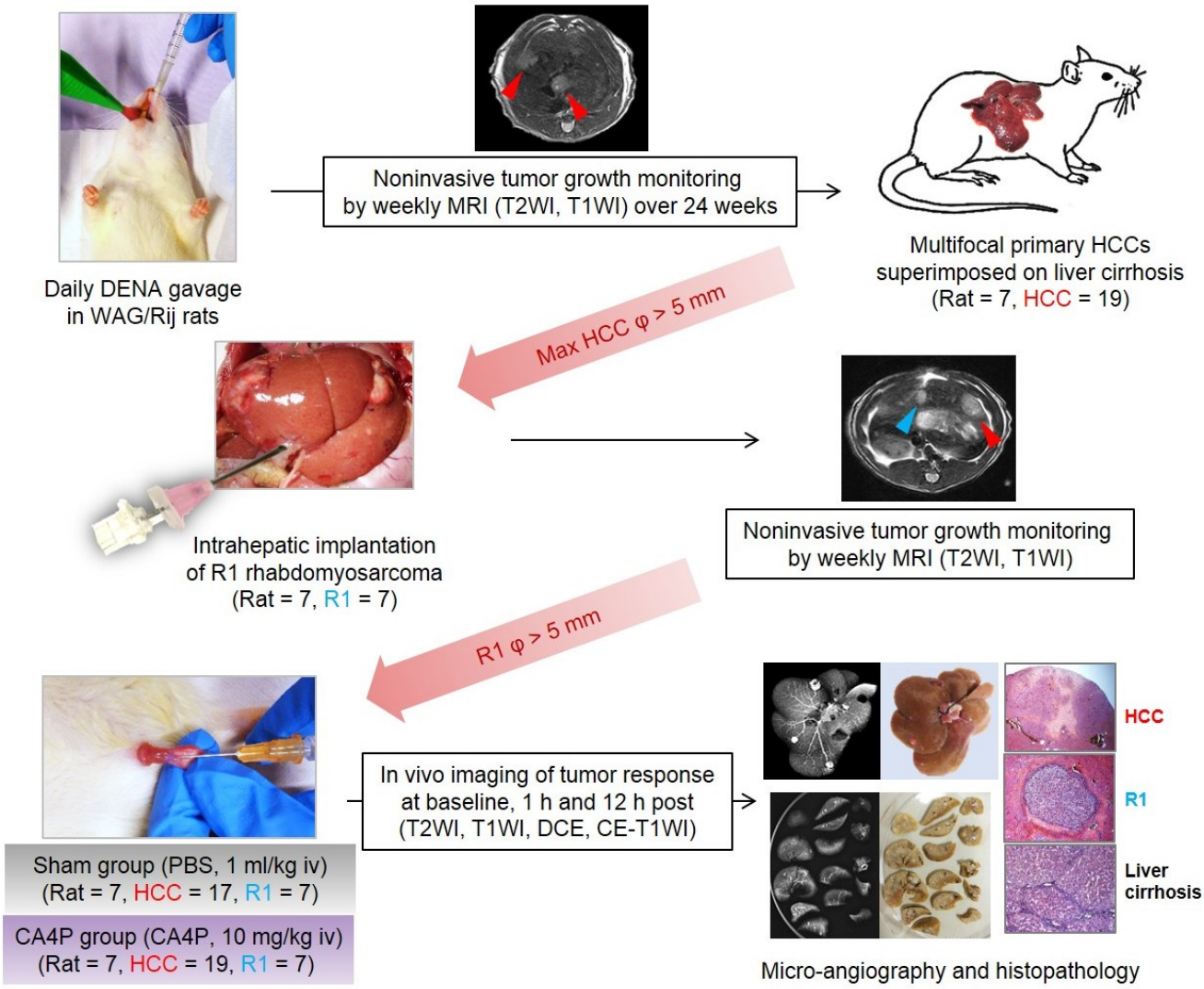

Figure 1. Flow chart of experimental protocol. DENA: diethylnitrosamine; WAG/Rij rat: Wistar Albino Glaxo/Rijswijk rat; MRI: magnetic resonance imaging; T2WI: T2-weighted imaging; T1WI: T1-weighted imaging; HCC: hepatocellular carcinoma; Ø: diameter; R1: R1 rhabdomyosarcoma; PBS: phosphate buffered saline; CA4P: combretastatin A4 phosphate; iv: intravenous(ly); h: hour; DCE: dynamic contrast enhanced; CE: contrast-enhanced.

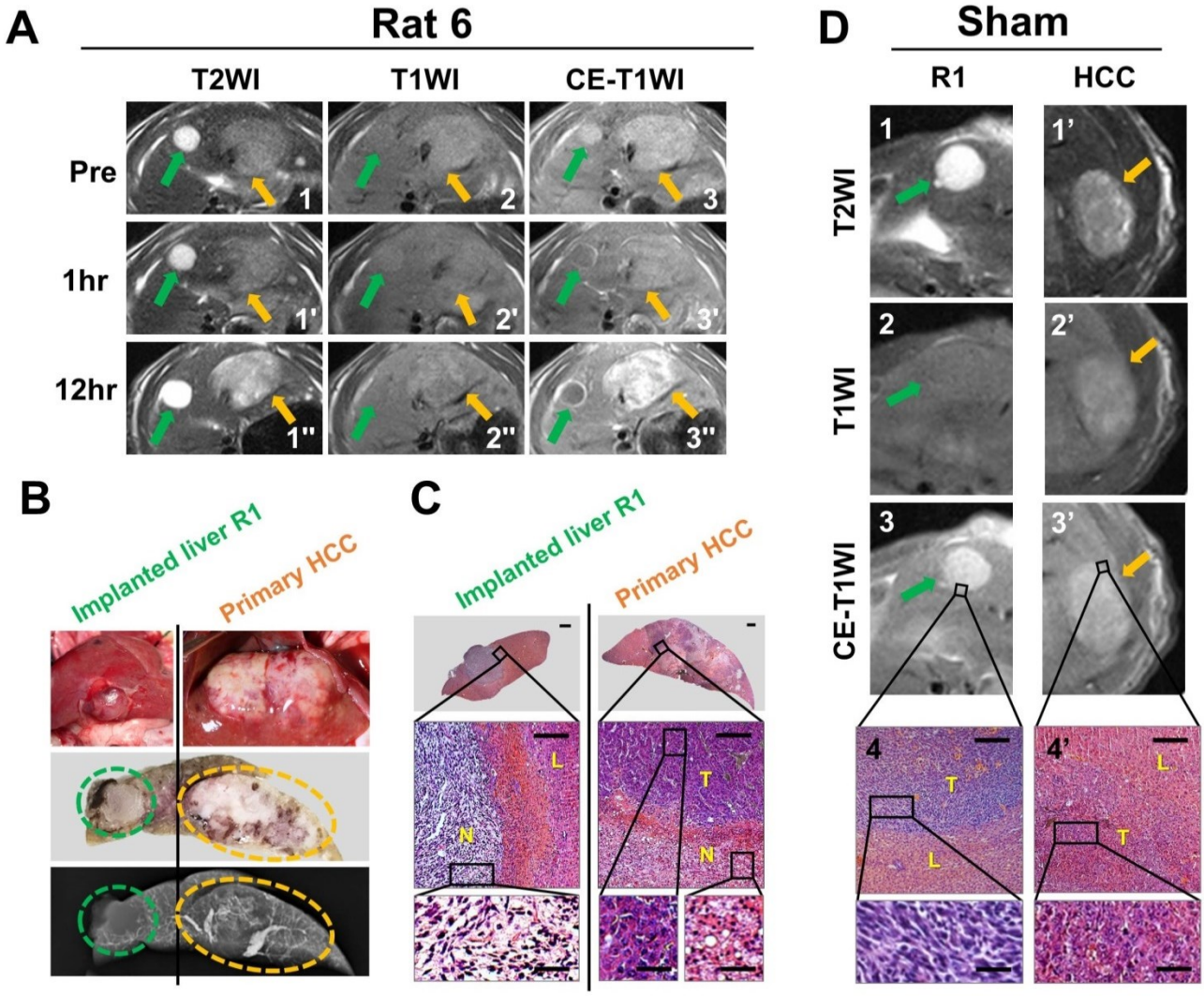

Figure 2. Intra-individual comparison of therapeutic responses to CA4P between a primary HCC and a hepatic R1 allograft located in different liver lobes. (A) T2WIs (1-1’’), T1WIs (2-2’) and CE-T1WIs (3-3’’) of an implanted R1 tumor (green arrows) and a primary HCC (orange arrows) located in the median and left liver lobes, respectively, at baseline and 1 h and 12 h post CA4P therapy. (B) Corresponding photomacrographs of median and left liver lobes (top panels), photomacrograph of liver blocks (median panel) in 2-mm thickness corresponding to the transversal MR images, and microangiogram (bottom panel) of tumor-bearing liver blocks, revealing 1 R1 tumor (green circle) and 1 primary HCC (orange circle). (C) Corresponding photomicrographs of R1 tumor (left column) and primary HCC (right column) in the median and left lobes, respectively. (H&E staining; upper panels, ×12.5 original magnification, scale bar = 800 μm; lower panels, ×100 original magnification, scale bar = 100 μm, ×400 original magnification, scale bar = 25 μm. N: tumoral necrosis; L: liver; viable tumor.). (D) Sham control: T2WIs (1, 1’), T1WIs (2, 2’) and CE-T1WIs (3, 3’) of R1 tumor (green arrows) and primary HCC (orange arrows) located in the median and left liver lobes, respectively, at 12 h post PBS treatment; and corresponding photomicrographs (4, 4’; H&E staining ×100 original magnification, scale bar = 100 μm, ×400 original magnification, scale bar = 25 μm. T: viable tumor; L: liver).

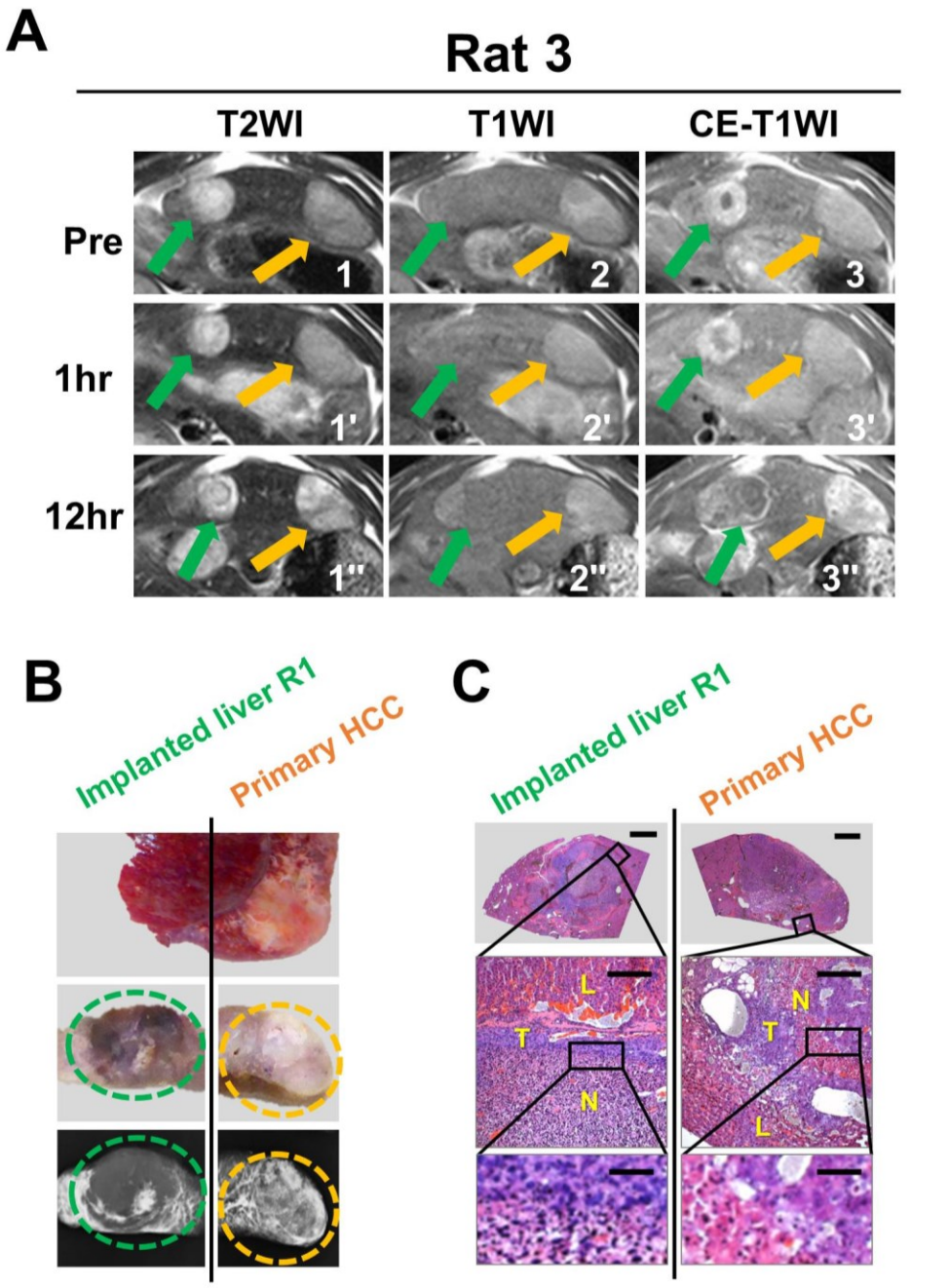

Figure 3. Intra-individual comparison of therapeutic responses to CA4P between a primary HCC and a hepatic R1 allograft distributed in the same liver lobe. (A) T2WIs (1-1’’), T1WIs (2-2’’) and CE-T1WIs (3-3’’) of an implanted R1 tumor (green arrows) and a primary HCC (orange arrows) both located in the same left liver lobe at baseline and 1 h and 12 h post CA4P therapy. (B) Corresponding macroscopic photographs of the left liver lobe (top panel) and liver blocks (median panels) in 2-mm thickness corresponding to the transversal MR images, and microangiograms (bottom panels) of tumor-bearing liver block, revealing a R1 tumor (green circle) and a primary HCC (orange circle). (C) Corresponding photomicrographs of R1 tumor (left column) and primary HCC (right column). (H&E staining; upper panels, ×12.5 original magnification, scale bar = 800 μm; lower panels, ×100 original magnification, scale bar = 100 μm, ×400 original magnification, scale bar = 25 μm. L: liver; T: viable tumor; N: tumoral necrosis.).

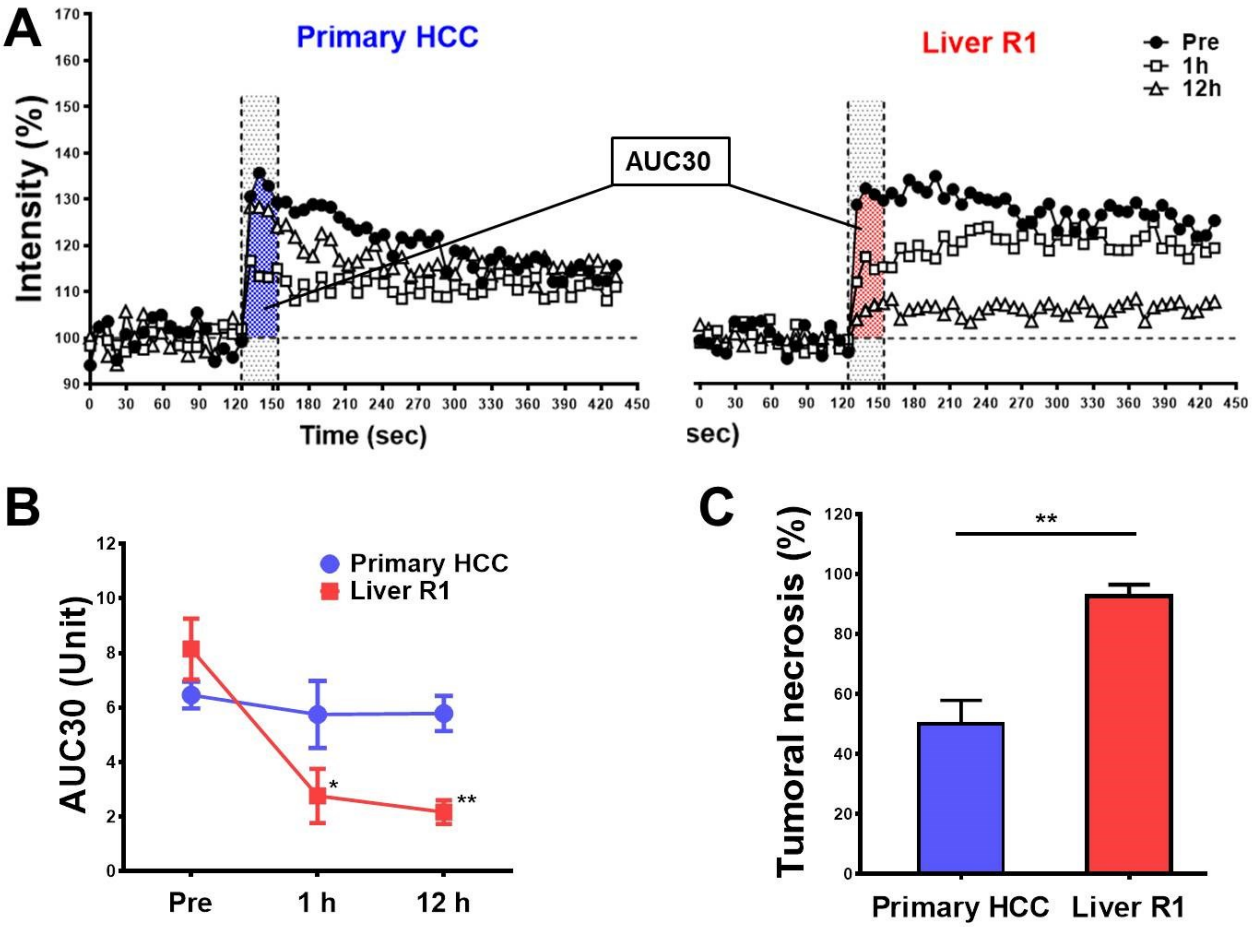

Figure 4. Changes of semi-quantitative DCE parameter of primary HCCs and implanted liver R1 tumors and quantification of CA4P-induced tumoral necrosis. (A) Representative contrast enhancement-time curves (CTCs) of a primary HCC and a secondary liver R1 tumo before, 1 and 12 h after CA4P treatment, for calculating tumor AUC30 at different time points. (B) Quantitative changes of tumor blood supply between HCCs and R1 tumors at baseline and 1 h and 12 h post CA4P treatment indicated by AUC30. (C) Bar chart compared the percentile tumoral necrosis between primary HCCs and implanted liver R1 at 12 h post CA4P therapy, which was estimated by post-mortem H&E staining (**P<0.01).